Journal of Applied Fluid Mechanics, Vol. 9, No. 2, pp. 537-542, 2016.
Available online at www.jafmonline.net, ISSN 1735-3572, EISSN 1735-3645.

Usability of the Selig S1223 Profile Airfoil as a High Lift Hydrofoil for Hydrokinetic Application

S. A. Oller[1†], L. G. Nallim[1] and S. Oller[2]

[1] *INIQUI – CONICET –Faculty of Engineering, National University of Salta, Salta, 4400, Argentina*
[2] *UPC-CIMNE – International Center for Method in Engineering, UPC Technical University of Catalonia (Barcelona Tech), Barcelona 08034*

†*Corresponding Author Email: sergio.oller@conicet.gov.ar*

(Received December 7, 2014; accepted March 4, 2015)

ABSTRACT

This work presents a numerical analysis of the ability of the high lift airfoil profile Selig S1223 for working as hydrofoil under water conditions. The geometry of the hydrofoil blade is designed through a suitable airfoil profile and then studied carefully by means of Computational Fluid Dynamics (CFD) in order to check its hydrodynamic behavior, i.e., including lift and drag analysis, and determinations of streamlines velocities and pressures fields. Finally conclusions on the use of this profile in a possible application for hydrokinetic turbine blades are detailed.

Keywords: Hydrofoil; Hydrokinetic generation; Computational Fluid Dynamics (CFD).

NOMENCLATURE

C	airfoil chord
c_y	lift coefficient
c_x	drag coefficient
F_{lift}	lift force
P	pressure
Re	Reynolds number
S_{wing}	wing surface
T	torque
t	time
v	absolute flow velocity
W	power
α_0	design attack angle
α	real angle of attack
α_{max}	maximum aerodynamic profile's α
η_v	velocity tolerance convergence error
η_P	pressure tolerance convergence error
ρ	fluid density
ω	angular velocity

1. INTRODUCTION

It is a fact the raise of the renewable energies requirements. Hydraulic energy is one of the more powerful ones, but the extremely high economic and environmental costs of the reservoirs constructions, turned the situation of these kinds of constructions around the world in a decreasing tendency.

Hydrokinetic turbines are an easier way of hydraulic energy usage due to the use of kinetic energy of current flow waters, instead of the reservoirs (Khan *et al.* 2008). Majority of the available published information concerns about WCT (Water Current Turbines) under marine tidal work conditions (Güney *et al*. 2010). Unfortunately, these kinds of rotors are useless on rivers because of their big size (4 – 8 times higher than a common river depth (Singh *et al*. 2014).

Majority of lowlands worldwide rivers, like the ones appearing in the *Major River Basins of the world* map (Fig.1) of the Global Runoff Data Centre (GRDC 2007), which is based on HYDRO1K system of the U.S Geological Survey (USGS), averages about 10m depth,and nearby $1.5\,\mathrm{m/s}$ ~$2\,\mathrm{m/s}$ of flow velocity (Hossein *et al*. 2012).So in hydrokinetic river operation (Khan and Bhuyan 2009),the efficiency of the hydrodynamic rotor is fundamental due to the low speed flows in fluvial beds, and the first efficiency step belongs to achieve a high performance hydrofoil´s design (Singh *et al*. 2014).

This work is motivated by the possibility of using inside water media flow, an airfoil profile capable of taking advantage of high lift efficiency, at low

flow speed operations. So the possibilities of using that kind of profile as the basis for hydrokinetic turbine blade design are explored.

Fig. 1. Major River Basins of the world.

2. HYDROFOIL SELECTION

From the viewpoint of engineering design, the more torque (T) has the turbine rotor, the more power (W) will develop the turbine, see Eq.(1). So, it is important to take advantage of the maximum possible torque and turbine's rotor velocity(ω) too.

$$W = T \cdot \omega \quad (1)$$

Torque and angular velocity of the rotor are achieved by airfoil's lift forces (Fig.2). Lift force depends on the change of pressures (ΔP) (Eq. (2)) generated in the airfoil surfaces, and these pressures depends on fluid density, airfoil shape profile and the airfoil angle of attackα (Eq. (3)) (Balaka and Rachman 2012).

$$\Delta P = P_{InnerSurface} - P_{OuterSurface} \quad (2)$$

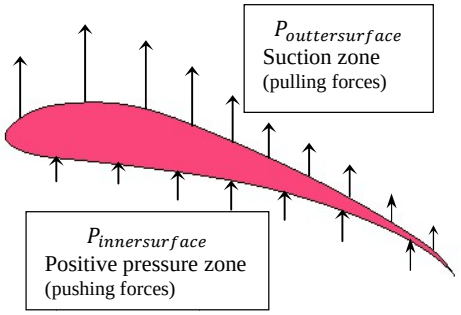

Fig. 2. Schematic representation of lift forces generated in a hydrofoil. Negative upper surface pressure (suction) and positive lower surface pressure.

If more lift is obtained by one airfoil, more torque (T) and angular velocity (ω) will be obtained by the turbine´s rotor. This commitment is achieved by selecting a high-lift aerodynamic shape profile for the hydrofoil design. The selected S1223 profile belongs to the high lift low Reynolds profiles class (Selig and Guglielmo1997) (see Fig.3). Under cambered airfoils, like S1223, have the best ratio of generating an extremely high lift at a minimum of flow velocity operation, and also this high lift is generated at very low angles of attack.

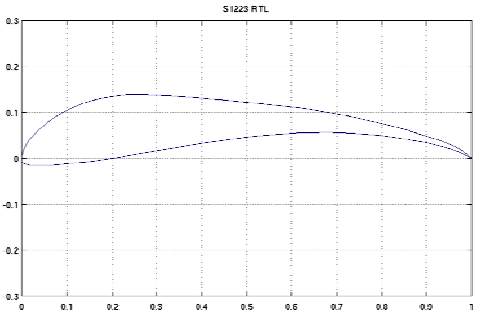

Fig. 3. Unitary normalized coordinates of S1223 airfoil generic profile.

University of Illinois wind tunnel measures a lift coefficient of $c_y = 2.2$ and drag coefficient $c_x = 0.046$ in a position of $\alpha = 10°$ of angle of attack, also measures the maximum attack angle of$\alpha_{max} = 15°$. Beyond that number boundary layer detachment flow will happen, dropping lift coefficient (Pengyin *et al*. 2014) and enormously increasing drag coefficient (Goundar *et al*. 2012).
Aerodynamics and Hydrodynamics disciplines are similar, but the study of the hydrodynamic requires taking care of ventilation and cavitation phenomenon. Turbine working in riverbed operation avoids the possibility of being affected by ventilation event. Cavitation is produced in the outer surface due to the low pressure of the incompressible fluid produced in its neighborhood; it depends on water temperature, airfoil profile and flow velocity. As higher the velocity is, higher the cavitation possibility.

3. MODEL GEOMETRY DESCRIPTION

Starting out from Michael S. Selig and James Gugliemo physical model (Selig and Guglielmo1997) (Fig.4), a similar three spatial finite element dimension numerical model is generated (Löhner. 2001) (Fig.5).

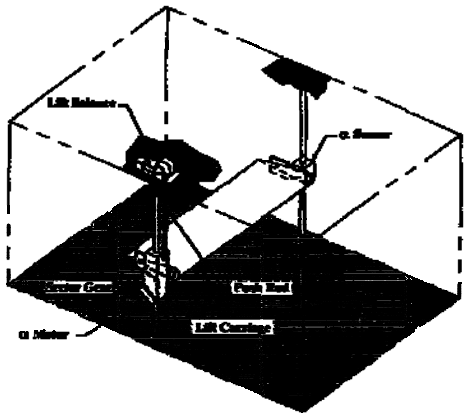

Fig. 4. Michael S. Selig and James Gugliemo physical model sketch (Selig and Guglielmo 1997).

The numerical model geometry consists on a hydrofoil made from a Selig´s S1223 profile, which

is located inside a cylindrical fluid control volume tunnel shape. Details and dimensions of this 0.2 m chord length (Pengyin *et al.* 2014) real scale numerical model can be observed in Fig.5, which shows a diametral-plane of the 3-D finite element model of the volume of control used for the numerical simulation.

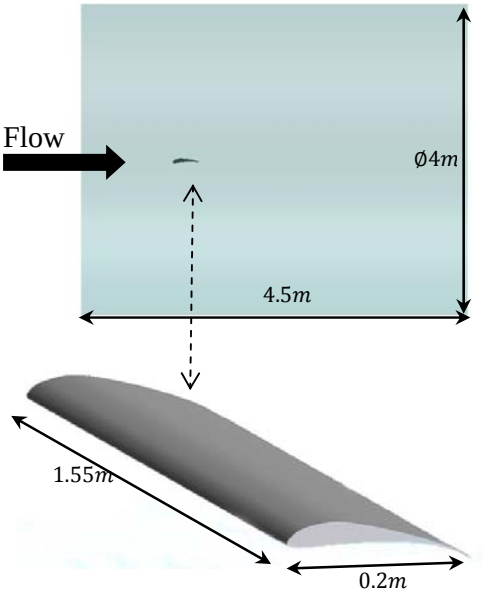

Fig. 5. Hydrofoil and 2-D diametral-plane scheme of the Volume of Control dimension of the 3-D numerical model geometry.

The bases of the difference between the numerical model presented, and the physical model, are the geometry of the volume of control and the fluid parameters. In numerical model a cylindrical volume of control is presented instead of the rectangular shape of the physical one, to avoid the influences of edges and corners in the fluid behavior. Also the push rod and airfoil anchors are not used, so it is ensured these elements will not affect the flow activity. Fluid parameters involve crossing the line from Selig and Guglielmo compressible flow essay, to a non-compressible numerical experiment, where the similitude between the lift coefficients must be ensured, but not this way the streamlines and more less the cavitation effect.

4. MODEL CONDITIONS, MESHING CRITERIA AND SOLVER

Since this work aims to analyze the ability of the mentioned profile operating like a hydrofoil device and not like airfoil one, fluid domain involves water conditions, so water parameters are given to fluid variables.

New validated Finite Element free open source multiphysics code *KRATOS* ("Kratos Multi-Physics". 2005) is used for the numerical simulation. The *Incompressible Fluid Application* of Kratos aims to solve the Navier-Stokes equations (see Eq. (3)). Instability of using linear FEM, are solved by different approaches like Fractional step or Subgrid scale stabilization (Codina. 2002).

Model conditions involve$v = 2\frac{\mathrm{m}}{\mathrm{s}}$ flow velocity iny axis positive direction, crossing the hydrofoil in axial form (Fig.5). Also, for all model surfaces, ano-slip condition of null velocity is applied.

Elapsed simulation time $\mathrm{t} = 1.5\mathrm{s}$ is used to ensure a state of steady flow achievement. Result drops unsteadily during th egap between $\mathrm{t}_0 = 0.0\mathrm{s}$ and $\mathrm{t}_\mathrm{u} = 0.4\mathrm{s}$, and beyond that point velocities and pressure stabilization occurs.

Incompressible problem type is solved using a bi-conjugate gradient stabilized (Van der Vorst. 1992) solver on velocity and pressure resolution. Convergence criterion reaches a maximum of 100 iterations involving velocity convergence error tolerance (η_v) and pressureconvergence error tolerance (η_P)of$\eta_\mathrm{v} = 1 \cdot 10^{-2} = \eta_\mathrm{P}$, using a$\Delta\mathrm{t}$ stabilization of$1 \cdot 10^{-3}\mathrm{s}$.

A Finite Element Variational Multiscale Simulation (FEVMS) (Hughes. 1995), (Guermond. 1999), (Hughes *et al*. 2000), method is applied to solve the grid, by the use of the general isothermal fluid Navier-Stokes governing equation for incompressible flow applications (Eq. (3)).

$$\rho\frac{\mathrm{D}\vec{\mathrm{v}}}{\mathrm{Dt}} = \rho\vec{\mathrm{g}} - \nabla\mathrm{p} + \mu\nabla^2\vec{\mathrm{v}} \qquad (3)$$

One point-one million of 4 nodes linear tetrahedicalfinite element (Zienkiewicz and Taylor 1991) (Lewis *et al*. 2004)isusedin a no structured volume mesh, and $1 \cdot 10^{-3}$cordal error is given as a strong tolerance to hydrofoil surface mesh.

5. MODEL VALIDATION UNDER AIR CONDITIONS

For the calibration of this model and sureness of its correct behavior, numerical model is also tested using air parameters instead of water ones. Numerical lift coefficient$c_y$obtained values are easily comparable with the experimental Michael S. Selig and James Gugliemo (Selig and Guglielmo1997) wind tunnel obtained values (Fig.6).

It can be observed the similitude of the ratio curve involving c_y relative toα, between experimental and numerical results model, maintaining less than 17%of average difference between both results. The qualitative shape of the numerical result is correct, and the difference observed in figure 6 for the obtained result is due to the influence of the cylindrical volume control (Fig. 5), chosen to avoid the edges and corners singularities, and also the wing position that has been chosen in the numerical test, instead of the actual volume chosen by M. S. Selig in the experimental test (Fig. 4). This features and results, also validates the use of the numerical model (FEM) presented in this work. Lift coefficient allows the obtaining of airfoil lift force

(Eq. (4)), and so this way curve comparison of lift forces are presented in Fig.7.

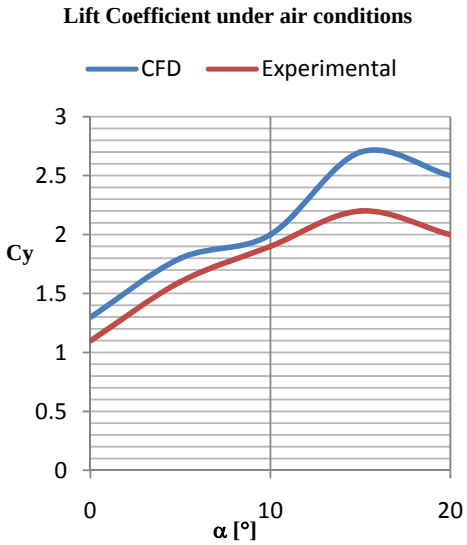

Fig. 6. Comparison of lift coefficients obtained by numerical results and wind tunnel.

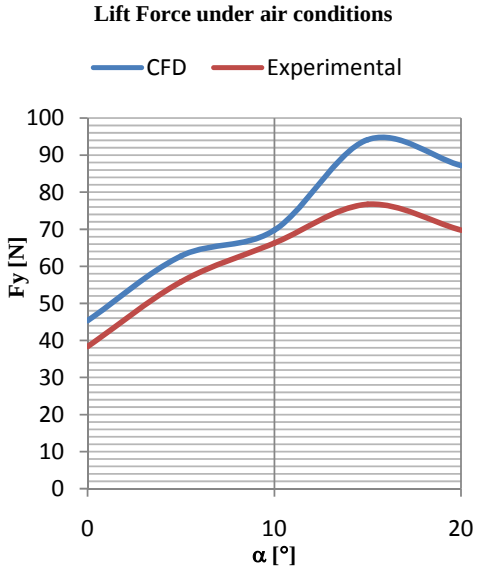

Fig.7. Lift force generated by airfoil in air fluid conditions.

6. HYDROFOIL RESULTS UNDER WATER CONDITIONS

Axial flow generates uniform pressure distribution along the hydrofoil wingspan surface (Fig.8, Fig.9) and is clearly visible the induced change of pressure ΔP formed in the flow field nearby the airfoil (Fig.10).

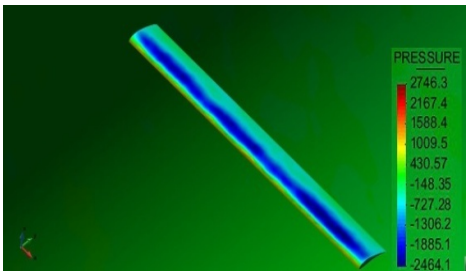

Fig. 8. Negative pressure distribution (suction) [Pa] generated on the hydrofoil upper surface. Figure corresponding to $\alpha = 10^{\circ}$.

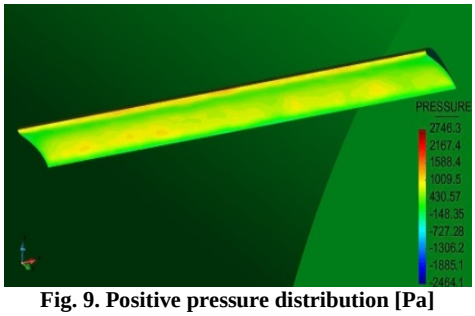

Fig. 9. Positive pressure distribution [Pa] generated on the hydrofoil lower surface. Figure corresponding to $\alpha = 10^{\circ}$.

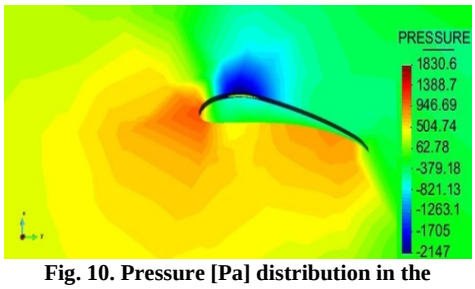

Fig. 10. Pressure [Pa] distribution in the hydrofoil surrounding flow field. Figure corresponding to $\alpha = 10^{\circ}$.

Stable streamlines along the entire Volume of Control field can be observed (Fig.11) in post process.

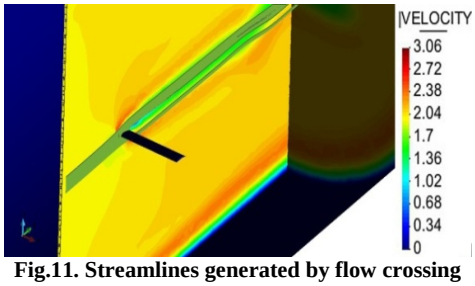

Fig.11. Streamlines generated by flow crossing the Volume of Control. Figure corresponding to $\alpha = 10^{\circ}$. Velocity units [m/s].

Starting out from the pressure (ΔP) generated in the inner and outer surface of the tested wing, is obtain lift force (F_{lift}) thru wingspan surface (S_{wing}). Fluid density (ρ) and flow velocity (v), complete the

necessary parameters to obtain the wing lift coefficient (c_y), calculated thru Eq. (4) as follows

$$c_y = \frac{F_{lift}}{\rho \cdot 0.5 \cdot v^2 \cdot S_{wing}} \quad (4)$$

Numerical model results show that lift force of profile S1223 airfoil is highly increased (Fig.12), reaching a maximum $F_{lift} = 1516$ Nat $\alpha = 15°$ in the usage of water fluid conditions, instead of the air fluid conditions initial designed for.

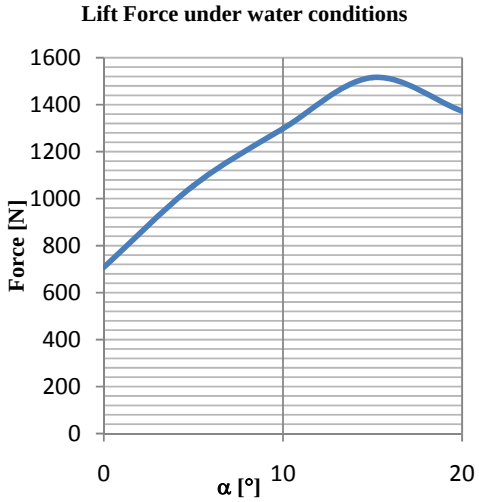

Fig. 12. Numerical lift for ceobtained under water conditions.

Figure 13 remarks the well boundary layer behavior, between the gap formed by $\alpha = 0°$ and $\alpha = 5°$ of angle of attack (Fig.13.a, Fig.13.b); and how detached flow becomes incipient at the angle of attack $\alpha = 10°$ (Fig.13.c) with a clearly growing tendency in $\alpha = 15°$ (Fig.13.d). Also, can be clearly observed in Figure 13.e, that beyond $\alpha = 20°$, full hydrofoil detached flow occurs. Detached flow changes the operating principle of the turbine, from lift operation to drag operation. Working on drag ambit decreases dramatically turbine efficiency. Detached flow also produces structural vibrations, which are especially dangerous to rotating airfoils with high aspect ratio.

Results show nearby 98861 Pa of absolute pressure in the outer foil surface, and cavitation phenomena occurs below 1250 Pa in 10 º C water, so it is possible to certify no cavitation phenomenon for the S1223 high lift profile, working at the detailed operation conditions.

7. CONCLUSION

The achievement of a free flow water turbine challenges the energy extraction belonging to a very low speed flow.

Classic water falls turbines operate at high flow speeds, so are not suitable for free flow stream. In hydrodynamics symmetrical profiles are commonly used to avoid cavitation, but as hydrokinetics free flow turbines operates at low speed flows, their blades have no needs of avoid cavitation, as well as is imperative to produce the highest lift possible just for the same reason of the low speed flow.

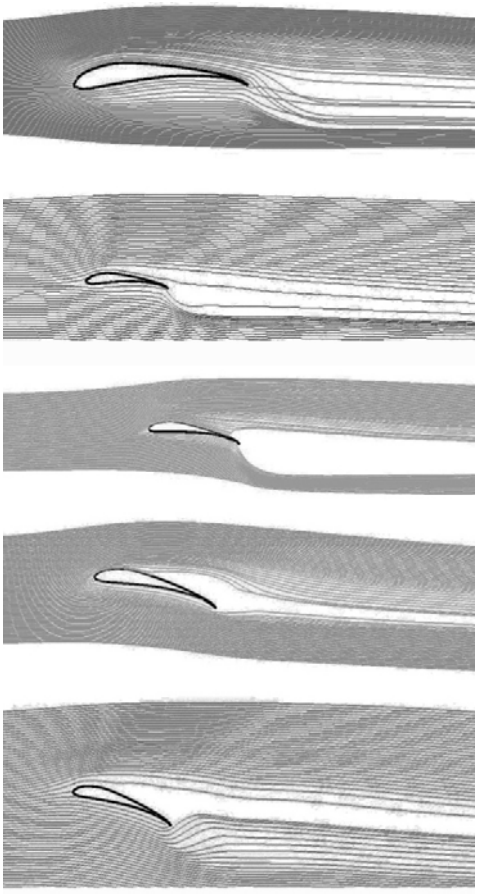

Fig. 13. Flow detachment evolution, from $\alpha = 0°$ (a), $\alpha = 5°$ (b), $\alpha = 10°$(c), $\alpha = 15°$ (d), to $\alpha = 20°$ (e).

Reaching $Re = 4.0 \cdot 10^5$ Reynolds number, this model discloses a good behavior in water fluid conditions, exposing right pressure distribution along the wingspan, and in the flow field, also proving not entering in cavitation zone. Similar to the original airfoil, this hydrofoil begins detaching flow at the angle of attack $\alpha = 10º$, reaching full detachment beyond $\alpha = 20º$.

Section 2 of this work explains the direct relationship existing between high efficient hydrofoil design achievements with the efficiency in hydrokinetic generation. Results achieved in this work evidence how suitable is the S1223 profile (aerodynamic initially designed for) at hydrodynamics tasks; and consequently, for the particular use of hydrokinetic turbine blade design.

This work can be used as starting point for a future design of a high performance hydrokinetic rotor thru their corresponding turbine blades.

ACKNOWLEDGEMENTS

This work has been supported by the Spanish Government through the Ministry of Science and Innovation (RECOMP project, ref. BIA2005-06952 and DELCOM Project, ref. MAT2008-02232); AECID (ref. A/024063/09) Spain; Barcelona Tech (Technical University of Catalonia UPC), Spain; International Center for Numerical Method in Engineering (CIMNE), Spain; CIMNE-Classrooms of National University of Salta, Argentina; Consejo Nacional de Investigación Científica y Técnica (CONICET), Argentina, and Consejo de Investigación de la Universidad Nacional de Salta (CIUNSa), Argentina. In addition, this work was partially supported by the European Research Council under the Advanced Grant: ERC-2012-AdG 320815 COMPDES-MAT. All this support is gratefully acknowledged.

REFERENCES

Balaka, R. and A. Rachman (2012).Pitch angle effect for horizontal axis river current turbine.*Procedia Engineering*, no. 50, 343-353.

Global Runoff Data Centre (GRDC) (2007). http://www.bafg.de/GRDC/EN/02_srvcs/22_gslrs/221_MRB/riverbasins_node.html .

Goundar, J. N., M. A. Rafiuddin and Y. H. Lee (2012).Numerical and experimental studies on hydrofoils for marine current turbines.*Renewable Energy*42, 173-179.

Guermond, J. (1999). Stabilization of Galerkin approximations of transport equations by subgrid modeling.*M2AN*33, 1293–1316.

Güney, M.S. and K. Kaygusuz (2010). Hydrokinetic energy conversion systems: A technology status review. *Renewable and Sustainable Energy Reviews* 14, 2996–3004.

Hossein, B., J. Woods and E. L. Bibeau (2012). Investigation of macro-turbulent flow structures interaction with a vertical hydrokinetic river turbine.*Renewable Energy*48, 183-192.

Hughes, T. (1995).Multiscale phenomena, Green's functions, the Dirichletto-Neumann formulation, subgrid-scale models, bubbles and the origin of stabilized methods.*Comput. Methods Appl. Mech. Eng.* 127, 387–401.

Hughes, T., L. Mazzei and J. Jansen (2000).Large Eddy simulation and the variationalmultiscalemethod.*Comput.Visual. Sci*. 3, 47–59.

Khan, M.J., G. Bhuyan, M. T. Iqbal and J. E. Quaicoe (2009). Hydrokinetic energy conversion systems and assessment of horizontal and vertical axis turbines for river and tidal applications: A technology status review.*Applied Energy*86, 1823-1835.

Khan, M.J., M. T. Iqbal and J. E. Quaicoe (2008). River current energy conversion systems: Progress, prospects and challenges.*Renewable and Sustainable Energy Reviews*12, 2177-2193.

Kratos Multi-Physics, CIMNE. (2000). [Online].Available

Lewis, R., P. Nithiarasuand K. Setharamu (2004).*Fundamentals of the finite element method for heat and finite element method for heat and fluid flow*.John Wiley and sons.

Löhner, R. (2001). Applied CFD Techniques: *An* Introduction Based on Finite Element Methods.John Wiley & Sons.

Pengyin, L., Y. Guohua, Z. Xiaocheng and D. Zhaohuix (2014).Unsteady aerodynamic prediction for dynamic stall of wind turbine airfoils with the reduced order modeling, *Renewable Energy*69, 402-409.

Selig, M. S. and J. J. Guglielmo (1997).High-Lift Low Reynolds Number Airfoil Design.*Journal of aircraft*34(1), 72-79.

Singh, P. M.andY. D. Choi (2014). Shape design and numerical analysis on a 1 MW tidal current turbine for the south-western coast of Korea.*Renewable Energy* 68, 485-493.

Van der Vorst, H. A. (1992). Bi-CGSTAB: A Fast and Smoothly Converging Variant of Bi-CG for the Solution of Nonsymmetric Linear Systems.*SIAM Journal on Scientific Computing* 13, 631–644.

Zienkiewicz, O. C. and L. R. Taylor (1991).*The finite element method*. London: McGraw-Hill.